Journal of Power Sources 196 (2011) 688–691

Contents lists available at ScienceDirect

Journal of Power Sources

journal homepage: www.elsevier.com/locate/jpowsour

Short communication

Fabrication and characterization of anode-supported micro-tubular solid oxide fuel cell based on $BaZr_{0.1}Ce_{0.7}Y_{0.1}Yb_{0.1}O_{3-\delta}$ electrolyte

Fei Zhao, Chao Jin, Chenghao Yang, Siwei Wang, Fanglin Chen*

Department of Mechanical Engineering, University of South Carolina, Columbia, SC 29208, USA

ARTICLE INFO

Article history:
Received 25 June 2010
Received in revised form 16 July 2010
Accepted 20 July 2010
Available online 30 July 2010

Keywords:
Solid oxide fuel cell
Micro-tubular
Proton conductor
Phase inversion

ABSTRACT

Anode-supported micro-tubular solid oxide fuel cells (SOFCs) based on a proton and oxide ion mixed conductor electrolyte, $BaZr_{0.1}Ce_{0.7}Y_{0.1}Yb_{0.1}O_{3-\delta}$ (BZCYYb), have been fabricated using phase inversion and dip-coating techniques with a co-firing process. The single cell is composed of NiO–BZCYYb anode, BZCYYb electrolyte and $La_{0.6}Sr_{0.4}Co_{0.2}Fe_{0.8}O_{3-\delta}$ (LSCF)–BZCYYb cathode. Maximum power densities of 0.08, 0.15, and 0.26 W cm^{-2} have been obtained at 500, 550 and 600 °C, respectively, using H_2 as fuel and ambient air as oxidant.

1. Introduction

Solid oxide fuel cells (SOFCs) have attracted interest as energy conversion devices because of their distinct advantages such as high thermodynamic efficiency, pollution-free operation and fuel flexibility [1,2]. Present development of SOFCs is focused on two major designs which can be classified as planar and tubular geometric configurations. Tubular SOFC systems have shown many advantages over the planar SOFCs, including higher mechanical robustness, better thermal-cycling behavior and simpler gas sealing [3–5]. Moreover, as the diameter of the tubular SOFC is decreased, it is possible to design micro-tubular SOFC stacks for high volumetric power density because this scales with the reciprocal of the tube diameter, as well as high thermal shock resistance which is in favor of quick start-up/shut-down.

In the past few years, traditional extrusion techniques have been normally used to fabricate the substrate tubes of the micro-tubular SOFCs [6–8]. Recently, a phase inversion method has been employed to fabricate electrolyte-supported micro-tubular SOFCs with conventional oxygen-ion conducting electrolytes such as yttria-stabilized zirconia (YSZ) and $Ce_{0.8}Sm_{0.2}O_{1.9}$ (SDC) [9,10]. Although a high open voltage of 1.2 V was obtained for the YSZ micro-tubular SOFC, its maximum power density was only about 0.018 W cm^{-2} at 800 °C because of the high electrolyte ohmic loss [9,11], which is noncompetitive for intermediate temperature SOFCs (IT-SOFCs). Therefore, reduction of the ohmic resistance is an urgent subject for micro-tubular cells operated at intermediate temperatures. It has been recently reported that $BaZr_{0.1}Ce_{0.7}Y_{0.1}Yb_{0.1}O_{3-\delta}$ (BZCYYb), a mixed proton and oxide ion conductor, exhibits higher conductivity over the traditional electrolytes such as YSZ, $Ce_{0.9}Gd_{0.1}O_{1.95}$ (GDC), and $BaZr_{0.1}Ce_{0.7}Y_{0.2}O_{3-\delta}$ (BZCY) at reduced operating temperatures (500–700 °C) [12]. The application of electrolyte material with high conductivity in SOFCs is an effective approach for reducing the ohmic loss and cost. In addition, an anode-supported cell allows a thin electrolyte to be deposited on the supporting anode, thus reducing the resistance losses from the electrolyte and yielding improved cell performance at reduced operating temperatures over an electrolyte-supported cell configuration. Consequently, anode-supported cell with thin film electrolyte can be considered as another promising approach to increase the performance of micro-tubular SOFC for operation at reduced temperatures.

Although micro-tubular SOFCs have been extensively reported recently [6–10,13,14], there has been no study on the fabrication and characterization of proton and oxide ion mixed conducting anode-supported micro-tubular cell for IT-SOFC applications. In this work, nickel and BZCYYb anode-supported micro-tubular SOFC based on BZCYYb electrolyte with an outer diameter (O.D.) less than 2 mm was fabricated by phase inversion and dip-coating techniques with a co-firing process. Electrochemical evaluation of the micro-tubular cell was performed in the temperature range 500–600 °C using humidified H_2 as fuel and ambient air as oxidant.

* Corresponding author. Tel.: +1 803 777 4875; fax: +1 803 777 0106.
E-mail address: chenfa@cec.sc.edu (F. Chen).

0378-7753/$ – see front matter © 2010 Elsevier B.V. All rights reserved.
doi:10.1016/j.jpowsour.2010.07.058

2. Experimental

2.1. Powder fabrication and characterization

The components of the micro-tubular SOFC were selected as follows: NiO–$BaZr_{0.1}Ce_{0.7}Y_{0.1}Yb_{0.1}O_{3-\delta}$ as an anode (support tube), BZCYYb as an electrolyte and $La_{0.6}Sr_{0.4}Co_{0.2}Fe_{0.8}O_{3-\delta}$ (LSCF)–BZCYYb as a cathode. NiO was synthesized by a glycine–nitrate process as previously reported [15]. BZCYYb powder was prepared by a sol–gel modified Pechini process [16]. In this process, ethylenediaminetetraacetic acid (EDTA) and citric acid were used as chelating and complexing agents, respectively. Ammonium hydroxide was added to promote the dissolution of EDTA in deionized water to form an aqueous solution of EDTA. An aqueous solution containing stoichiometric amounts of barium, zirconium, cerium, yttrium and ytterbium nitrate salts was subsequently slowly added to the aqueous EDTA solution. Finally, an appropriate amount of citric acid was added (citric acid:metal nitrates:EDTA molar ratio = 1.5:1:1) and the final solution was stirred at room temperature for 24 h. Water was then slowly evaporated on a hot plate and the resulting brown gel was dried at 300 °C. The dried ash was then placed in an alumina crucible and fired in a muffle furnace at 1100 °C for 6 h in air to achieve fine BZCYYb powder. Phase analysis of the samples was performed on a Mini X-ray diffractometer using Cu Kα radiation (λ = 0.15418 nm), employing a scanning rate of 10 ° min^{-1} in the 2θ range of 20–80°.

2.2. Micro-tubular cell fabrication and characterization

Micro-tubular anode substrate was fabricated by using a phase inversion method [17]. NiO, BZCYYb and graphite powders with a weight ratio of 65:35:10 were mixed with ethanol by ball milling for 24 h and then dried. The as-prepared mixture was subsequently mixed with polythersulfone (PESf) and *N*-methyl-2-pyrrolidone (NMP) to form a viscous slurry. A custom designed spinneret with an orifice dimension/inner diameter of 3.0/2.0 mm was used to obtain a micro-tubular precursor (MTP). The MTP was then immersed into a water bath (25 °C) for 30 min to perform water molecules-spinning solution molecules exchange process, resulting in a porous MTP. The porous MTP was washed with deionized water for several times to remove excess solvent, dried at 400 °C for 2 h to remove organic binder, and then fired at 1200 °C for 2 h. A thin BZCYYb electrolyte membrane was then coated onto the pre-fired NiO–BZCYYb micro-tubular anode substrate with a dip-coating method using a similar BZCYYb suspension as described previously [18]. After co-firing at 1400 °C for 5 h in air, a dense BZCYYb electrolyte film with a thickness of 25 μm on the porous NiO–BZCYYb micro-tubular anode substrate was obtained. Cathode slurry consisting of LSCF, BZCYYb and a binder (V-006, Heraeus) with a mass ratio of 7:3:15 was applied onto the surface of the tubular cell with a screen-printing method, followed by firing at 1100 °C for 2 h to form a complete tubular cell with an outer diameter of 1.6 mm for electrochemical testing. The thickness of the cathode was approximately 50 μm and the effective area of the cathode was 0.65 cm^2.

Ag paste (Heraeus, component metallization C8829) was used for collecting current from anode and cathode. Ag wire was attached to the inner wall surface of the anode-supported tube for collecting current from the anode side and wound around the outer surface of cathode. The anode-supported tubular SOFC was sealed by two alumina tubes with a ceramic bond (Ceramabond 552). The anode side was exposed to humidified hydrogen (3 vol% H_2O) with a flow rate of 30 mL min^{-1} while the cathode was exposed to ambient air. The cell current and voltage characteristics were evaluated in the temperature range of 500–600 °C. Impedance measurement was performed for the cell under open-circuit conditions with the applied frequencies in the range of 0.01 Hz to 1 MHz with a signal amplitude of 10 mV. The electrochemical test was performed using a Versa STAT3-400 electrochemical station. Structural investigation of tubular cell was carried out using a FEI Quanta-XL 30 model scanning electron microscope (SEM).

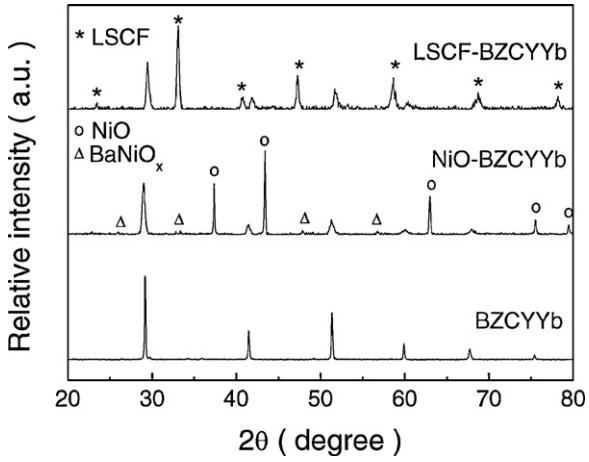

Fig. 1. X-ray diffraction patterns of BZCYYb electrolyte, NiO–BZCYYb anode and LSCF–BZCYYb cathode.

3. Results and discussion

3.1. Phase analysis

As shown in Fig. 1, the BZCYYb electrolyte film after co-sintering with NiO–BZCYYb anode at 1400 °C for 5 h can be identified as perovskite phase, which is in good agreement with the literature result [12]. Some minor peaks corresponding to barium nickel oxide ($BaNiO_x$) are found in the XRD spectrum for the co-sintered NiO–BZCYYb, indicating that trace amount of solid solution between NiO and doped barium cerate might be formed during the high co-sintering process. The XRD peaks of LSCF–BZCYYb cathode after firing at 1100 °C for 2 h are also shown in Fig. 1. There are no obvious peaks attributable to impurities, indicating that there are negligible interactions between LSCF and BZCYYb during the cathode fabrication process.

3.2. Microstructure of the micro-tubular cell

Cross-sectional SEM images of the anode-supported micro-tubular cell after testing are presented in Fig. 2. As shown in Fig. 2(1) the thickness of the anode is about 200 μm and BZCYYb electrolyte film with a thickness of 25 μm was successfully obtained on the anode tube by dip-coating and co-sintering method. Fig. 2(2) reveals that the electrolyte is dense and free of cracks, adhering very well to the Ni–BZCYYb anode layer. As shown in Fig. 2(3), uniform porous nickel and BZCYYb composite anode microstructures are formed, providing efficient channel for transporting the fuel gas as well as continuous ionic and electronic conducting paths.

3.3. Electrochemical performance of the micro-tubular SOFC

The performance of the micro-tubular cell was evaluated by measuring the polarization characteristics of the cell from 500 to 600 °C with humidified H_2 as fuel and ambient air as oxidant. As shown in Fig. 3(1), maximum power densities of 0.08, 0.15, and 0.26 W cm^{-2} with the OCV values of 1.05, 1.03 and 1.01 V were obtained at 500, 550 and 600 °C, respectively, which are much higher than those of the electrolyte-supported micro-tubular cells using YSZ as electrolyte (0.002 W cm^{-2} at 600 °C) [9] and

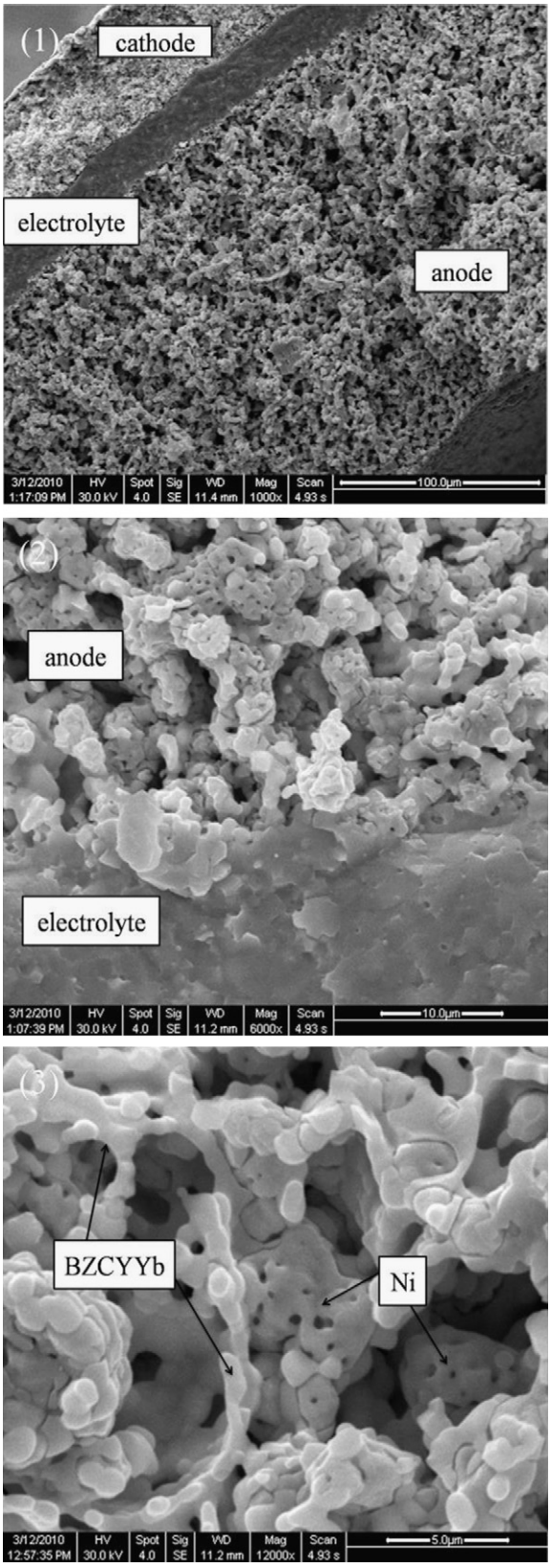

Fig. 2. Cross-section SEM images of (1) Ø 1.6 mm micro-tubular SOFC, (2) the electrolyte–anode interface, and (3) porous anode after tests.

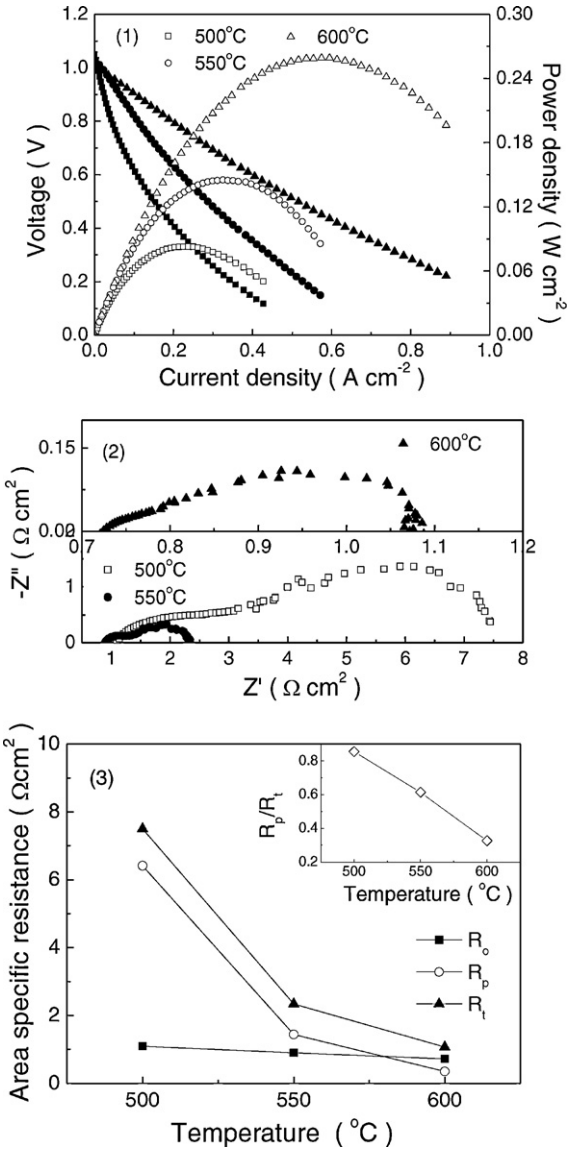

Fig. 3. Performance of the Ni–BZCYYb|BZCYYb|LSCF–BZCYYb micro-tubular cell. (1) Cell voltage and power density as a function of current density, (2) impedance spectra at different temperatures measured under open-circuit conditions, and (3) the total cell resistance (R_t), interfacial polarization resistance (R_p), and ohmic resistance (R_o) as determined from the impedance spectra as shown in (2). R_p/R_t is also shown in the figure.

SDC as electrolyte (0.045 W cm^{-2} at 600 °C) [10]. These results suggest that the cell performance is very promising and the electrolyte film is sufficiently dense, consistent with the SEM results shown in Fig. 2(2). The higher peak power densities are probably due to the use of the electrolyte with higher conductivity and much thinner electrolyte film, resulting in a significant reduction in the ohmic polarization from the electrolyte. Fig. 3(2) displays the impedance spectra of the micro-tubular cell measured under open-circuit conditions at different temperatures. The low frequency intercept corresponds to the total resistance (R_t), including ohmic resistance (R_o) and interfacial polarization resistance (R_p). The high frequency intercept represents R_o of the cell, involving ionic resistance of the electrolyte and electronic resistance of the electrodes [19]. The difference between the high frequency and low frequency intercepts with the real axis represents the total R_p of the cell, including the cathode–electrolyte interfacial resistance and the anode–electrolyte interfacial resistance [1]. The ohmic,

polarization and total resistances obtained from the impedance spectra are summarized in Fig. 3(3). As expected, the increase of the measuring temperature resulted in a significant reduction of the interfacial polarization resistances as shown in Fig. 3(3), typically from 6.41 $\Omega\,cm^2$ at 500 °C to 0.35 $\Omega\,cm^2$ at 600 °C. Further analysis shows that the ratio of R_p to R_t decreases with the increase in the cell operating temperatures, from 85.5% at 500 °C to 32.6% at 600 °C, indicating that the cell performance is significantly limited by R_p at low temperatures. Fig. 3 (3) further shows that R_t is mainly dominated by R_p at or below 550 °C while it is mainly dominated by R_o above 550 °C. Generally speaking, the performance of an SOFC strongly depends on the cathode–electrolyte interface at lower temperatures, since cathode interfacial polarization resistance increases rapidly with the decrease in the operating temperatures. The large R_p value observed in this work implies that electrochemical activity of LSCF cathode is not sufficient at low temperatures, consistent with previous reports [20,21]. Therefore, the cell performances may be further improved by using electrodes with better catalytic performance such as $Ba_{0.5}Sr_{0.5}Co_{0.8}Fe_{0.2}O_{3-\delta}$ (BSCF) [22] and optimizing the electrode microstructure to decrease the electrode polarization.

4. Conclusions

An anode-supported micro-tubular SOFC based on a proton and oxide ion mixed conductor, BZCYYb, was fabricated by using phase inversion and dip-coating techniques with a co-firing process. The cell configuration was composed of NiO–BZCYYb, BZCYYb and LSCF–BZCYYb as anode, electrolyte and cathode, respectively. The electrolyte is dense and free of cracks, and adheres very well to the anode layer. Maximum power densities of 0.08, 0.15, and 0.26 $W\,cm^{-2}$ with the OCV values of 1.05, 1.03 and 1.01 V were obtained at 500, 550 and 600 °C, respectively. The increase of the measuring temperature resulted in a significant reduction of the interfacial polarization resistances, typically from 6.41 $\Omega\,cm^2$ at 500 °C to 0.35 $\Omega\,cm^2$ at 600 °C.

Acknowledgement

The financial support of the Department of Energy NEUP (award no. 09-510) is acknowledged gratefully.

References

[1] N.Q. Minh, J. Am. Ceram. Soc. 76 (1993) 563.
[2] S.M. Haile, Acta Mater. 51 (2003) 5981.
[3] Y. Liu, S.I. Hashimoto, H. Nishino, K. Takei, M. Mori, T. Suzuki, Y. Funahashi, J. Power Sources 174 (2007) 95.
[4] A.V. Akkaya, Int. J. Energy Res. 31 (2007) 79.
[5] J. Jia, R. Jiang, S. Shen, A. Abudula, Environ. Energy Eng. 54 (2008) 554.
[6] T. Yamaguchi, S. Shimizu, T. Suzuki, Y. Fujishiro, M. Awano, Mater. Lett. 62 (2008) 1518.
[7] Y. Funahashi, T. Shimamori, T. Suzuki, Y. Fujishiro, M. Awano, J. Power Sources 163 (2007) 731.
[8] T. Suzuki, Y. Funahashi, T. Yamaguchi, Y. Fujishiro, M. Awano, J. Alloys Compd. 451 (2008) 632.
[9] C.C. Wei, K. Li, Ind. Eng. Chem. Res. 47 (2008) 1506.
[10] N.T. Yang, X.Y. Tan, Z.F. Ma, A. Thursfield, J. Am. Ceram. Soc. 92 (2009) 2544.
[11] C.J. Li, C.X. Li, Y.Z. Xing, M. Gao, G.J. Yang, Solid State Ionics 177 (2006) 2065.
[12] L. Yang, S.Z. Wang, K. Blinn, M.F. Liu, Z. Liu, Z. Cheng, M.L. Liu, Science 326 (2009) 126.
[13] T. Suzuki, T. Yamaguchi, Y. Fujishiro, M. Awano, J. Power Sources 160 (2006) 73.
[14] F. Calise, G. Restucccia, N. Sammes, J. Power Sources 195 (2010) 1163.
[15] F. Zhao, Z.Y. Wang, M.F. Liu, L. Zhang, C.R. Xia, F. Chen, J. Power Sources 185 (2008) 13.
[16] F. Zhao, Q. Liu, S.W. Wang, K. Brinkman, F. Chen, Int. J. Hydrogen Energy 35 (2010) 4258.
[17] C.H. Yang, C. Jin, F. Chen, Electrochem. Commun. 12 (2010) 657.
[18] F. Zhao, S.W. Wang, K. Brinkman, F. Chen, J. Power Sources 195 (2010) 5468.
[19] C.R. Xia, M.L. Liu, Adv. Mater. 14 (2002) 521.
[20] J. Kuhn, P. Matter, J. Millet, R. Watson, U. Ozkan, J. Phys. Chem. C 112 (2008) 12468.
[21] A. Esquirol, N.P. Brandon, J.A. Kilner, M. Mogensen, J. Electrochem. Soc. 151 (2004) A1847.
[22] Z.P. Shao, S.M. Haile, Nature 431 (2004) 170.